Materials Advances

ROYAL SOCIETY OF CHEMISTRY

PAPER

View Article Online
View Journal | View Issue

Cite this: *Mater. Adv.*, 2023, 4, 6612

Full-color emission of fluorinated benzothiadiazole-based D–A–D fluorophores and their bioimaging applications†

Si-Hong Chen,[a] Xi-Ying Cao,[a] Peng-Tao Hu,[a] Kai Jiang,*[b] Yong-Tong Liang,[a] Bing-Jia Xu,[a] Zhong-Hao Li[a] and Zhao-Yang Wang*[ab]

There is an active demand for full-color fluorophores in the field of fluorescent dyes. However, a core skeleton with a simple structure and easy modification is currently insufficient. Herein, we develop a range of full-color-tunable fluorophores **3a–3m** based on the fluorinated benzothiadiazole skeleton and their control compounds **3n–3p**. By regulating the charge transfer strength between donors and acceptors, the emission colors of **3a–3p** spanning from blue to red (λ_{em} = 445–672 nm) are achieved. Interestingly, compounds **3a–3p** with a fluorinated core skeleton exhibit sensitive solvatochromism effects, large Stokes shifts and excellent dual-state emission (especially **3c–3k**). Meanwhile, with the control of different substituents in the donor structure, ACQgens (**3a–3i** and **3n–3p**) can be facilely tuned to AIEEgens (**3j–3m**). Notably, red AIEEgen **3m** shows great potential for bioimaging in live cells with low cytotoxicity.

Received 18th October 2023,
Accepted 10th November 2023

DOI: 10.1039/d3ma00876b

rsc.li/materials-advances

Introduction

Full-color fluorophores can emit across the whole visible light spectrum (390–760 nm) by varying substituents of the core scaffold.[1,2] The tunable structure and photophysical properties of full-color fluorophores give them potential for a wide range of applications in sensing, bioimaging and organic light-emitting diodes (OLEDs).[3] Among them, as representatives of multicolor luminophores, quantum dots and carbon dots have attracted enormous attention owing to their high quantum yield (Φ_F) and color purity.[4] However, they still have some disadvantages, *e.g.*, an unclear luminescence mechanism and an ambiguous structure–property relationship, resulting in a narrow spectral range and difficulty in achieving solid-state emission.[5] Thus, many research groups have developed plenty of full-visible color-tunable organic fluorophores based on donor–acceptor (D–A) systems.[6,7]

For example, Yasuda *et al.* synthesized five D–A–D type full-color delayed fluorescent materials by making a central phthalonitrile or 2,3-dicyanopyrazine acceptor core that is connected with various donor units.[8] In 2023, Sun *et al.* developed eight carbazole-based D–D–A type full-color aggregation induced emission luminogens (AIEgens).[9] Recently, Samanta *et al.* reported a series of D–A–D type full-color pyrylium, pyridinium and pyridine derivatives and used them for pH imaging during mitophagy (Scheme 1i).[10] Nevertheless, the current skeletons are still inadequate for preparing advanced fluorescent materials. Some may have shortcomings of a narrow emission range

[a] *School of Chemistry, South China Normal University, Key Laboratory of Theoretical Chemistry of Environment, Ministry of Education, Guangzhou Key Laboratory of Analytical Chemistry for Biomedicine, GDMPA Key Laboratory for Process Control and Quality Evaluation of Chiral Pharmaceuticals, Guangzhou 510006, P. R. China. E-mail: wangzy@scnu.edu.cn, bingjiaxu@m.scnu.edu.cn; Tel: +8620-39310258*

[b] *Key Laboratory of Functional Molecular Engineering of Guangdong Province, South China University of Technology, Guangzhou 510640, P. R. China. E-mail: 201910104301@mail.scut.edu.cn*

† Electronic supplementary information (ESI) available: Instrumentation details; synthesis; characterization, including ^{1}H, ^{13}C, ^{19}F NMR, HRMS, and single crystal X-ray analysis; theoretical calculation analyses; TG analyses; UV-vis and fluorescence spectra; and bioimaging details (PDF). CCDC 2282710, 2282714, 2282717 and 2282718. For ESI and crystallographic data in CIF or other electronic format see DOI: https://doi.org/10.1039/d3ma00876b

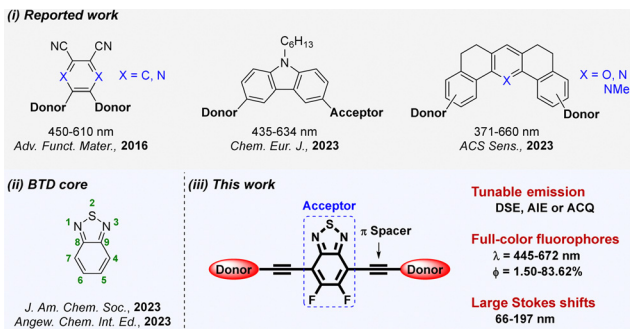

Scheme 1 An overview of full-color compounds *vs.* this work.

and single fluorescence performance. Hence, it is highly desirable but challenging to select a key core skeleton to design functional fluorophores with full-visible color tunability, and further explore their applications in the field of cell imaging.

Benzothiadiazole (BTD) is an important acceptor, and its derivatives have high fluorescence Φ_F, outstanding chemical and photostability, excellent aromaticity, and multiple modifiable sites. Meanwhile, it easily results in full-color fluorophores with tunable emission spectra from blue to red regions *via* incorporating diverse electron-donating units or extending the π-conjugated skeleton.[11,12] In recent reports, the BTD core has been successfully used;[13] especially, it can be developed into full-color metal–organic frameworks[14,15] or AIEgens[16] (Scheme 1(ii)). Although used as a building block with more electron-withdrawing nature,[17,18] 5,6-difluoro-BTD (FBTD) has not been systematically exploited for multifunctional luminophores with full-color emission (Scheme 1(iii)). In order to develop a variety of FBTD derivatives, this work is the first to construct a series of multifunctional full-color fluorophores based on a central FBTD core.

Modulating the charge transfer process and the molecular conformation of the D–A system has been a key strategy for successfully constructing full-color fluorophores with emission that can cover the whole visible region.[19,20] Among the detailed methods, fluorination may increase intra-molecular D–A interactions[21] and simultaneously enhance Φ_F in solid and solution states.[22] The alkynyl group as a π bridge can not only enhance the rigid conjugation of the intermediate skeleton, but also promote the free rotation of the units at both ends.[23] Meanwhile, dual-state emission (DSE) fluorophores, aggregation caused quenching (ACQ) luminogens and AIEgens have their own advantages in solution, aggregated and solid-state emissions,[24] and it is of great significance to realize the effective conversion of the three in the same framework. Therefore, the FBTD core is decorated with diverse donors *via* an acetylene linker, successfully making a series of D–A–D type full-color fluorophores **3a–3m** and their control compounds **3n–3p** (Fig. 1) are synthesized. These compounds not only have multifarious emission properties such as solvatochromism, DSE, ACQ and aggregation induced enhanced emission (AIEE) effects, but also have a wide emission range (445–672 nm), tunable fluorescence Φ_F (0.2–93%) and a large Stokes shift ($2.3 \times 10^3 - 6.8 \times 10^3$ cm^{-1}), which can basically overcome the many existing limitations of common fluorophores. More importantly, red emitter **3m** has low cytotoxicity and is successfully used for cell imaging.

Results and discussion

Synthesis and characterization of compounds 3a–3p

In this work, the synthesis routes of these full-color fluorophores **3a–3p** are shown in Schemes S1–S3 in the ESI.† Among them, **3a–3m** as the anticipated target compounds were successfully synthesized by the Sonogashira coupling reaction[25] of 4,7-dibromo-FBTD **1a** and terminal alkynes **2** with good yields

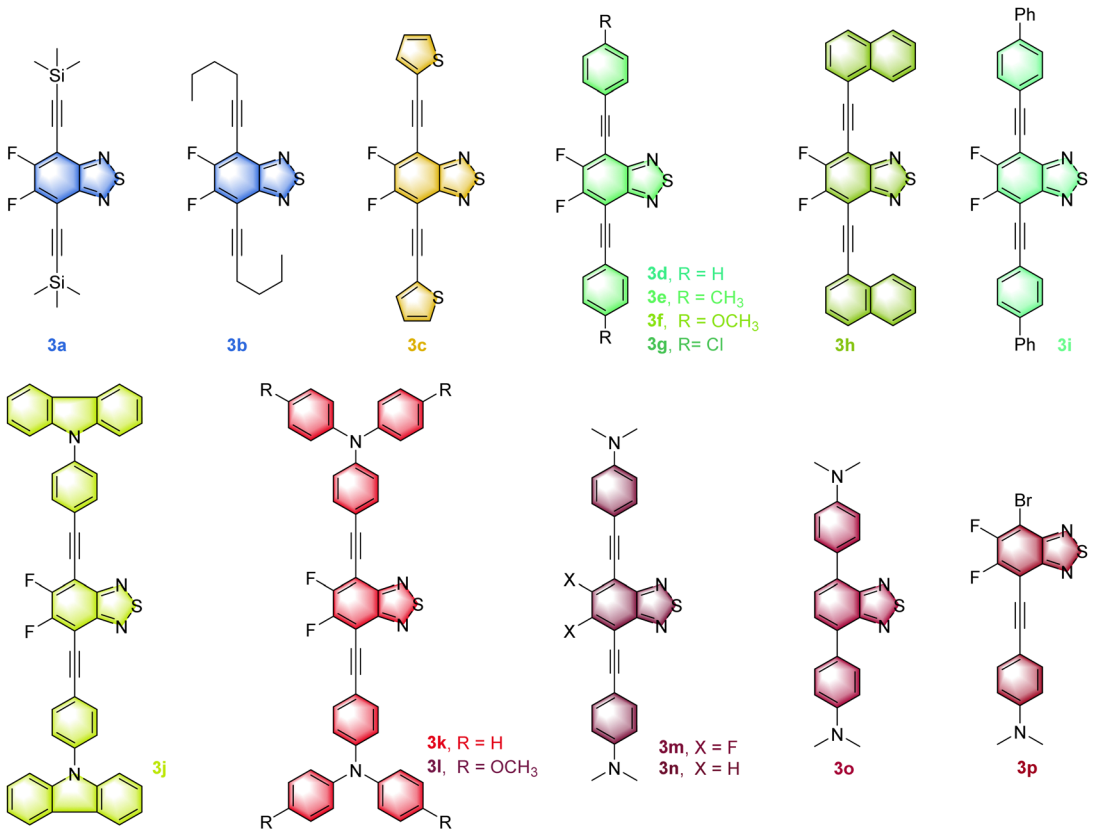

Fig. 1 Chemical structures of full-color fluorophores **3a–3p**.

(65–85%). It is shown that the electron-rich terminal alkynes are more conducive to the coupling reaction.

Accordingly, three control compounds **3n–3p** were synthesized by changing the reactant, reaction type or feeding ratio. For instance, **3n** is synthesized from 4,7-dibromo-BTD **1b** and 4-ethynyl-*N*,*N*-dimethylaniline **2m** by the Sonogashira reaction. **3o** is obtained by the Suzuki reaction[26] using 4,7-diborate-BTD **1′** and 4-bromo-*N*,*N*-dimethylaniline **2′**. When the molar ratio of **1a** and **2m** was controlled as 1 : 1, the monosubstituted compound **3p** was obtained by the Sonogashira reaction. Importantly, the molecular structure and purity of all obtained **3a–3p** were well demonstrated by ^{1}H, ^{19}F, ^{13}C NMR,[27,28] HRMS (Fig. S1–S62, ESI†) and single-crystal X-ray diffraction analysis (for compounds **3e**, **3f**, **3m** and **3p**, Tables S1–S4, Fig. S63 in the ESI†).

Thermal stability of compounds 3a–3p

The excellent thermal stability of the fluorophore molecules is an important prerequisite for the development of their fluorescence applications. Hence, a thermogravimetric analysis is performed on these new compounds and the decomposition temperature (T_d) is defined as the temperature at which weight loss is 5%.

As shown in Fig. S64 (ESI†), all of the T_d of compounds **3a–3p** are greater than 190 °C, indicating that these compounds have good thermal stability. Furthermore, the T_d of **3j** and **3k** is above 470 °C, and it may be due to that carbazole and triphenylamine (TPA) units have more benzene rings to disperse π electron density and reduce molecular energy. Compound **3n** presents the high T_d, which may be attributed to that the bond energy of C–F is greater than that of C–H.

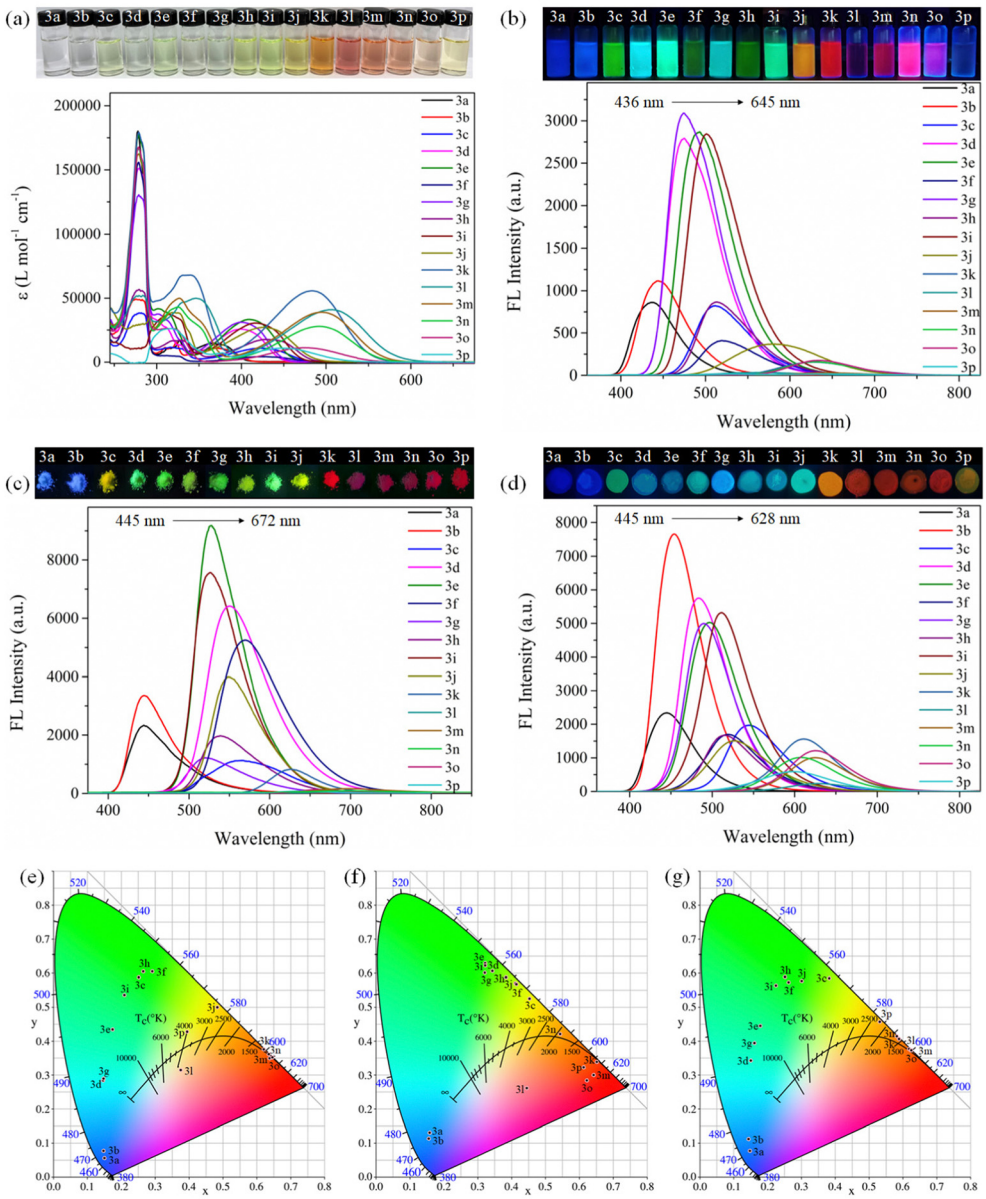

Fig. 2 (a) The UV-vis absorption spectra and photographs of compounds **3a–3p** in THF (10^{-5} M). (b) The fluorescence spectra and photographs of **3a–3p** in THF and (c) solid and (d) film states. The CIE chromaticity coordinates of **3a–3p** (e) in THF and (f) solid and (g) film states.

Photophysical properties of compounds 3a–3p

Dual-state emission. Firstly, the UV-vis absorption spectra of compounds **3a–3p** are tested in THF. As shown in Fig. 2a and Table 1, the absorption peaks of **3a–3p** are located at 270–510 nm. Meanwhile, they exhibit different colors in sunlight, including colorless, yellow-green, yellow, orange and red, which may be related to the strength of the intramolecular push–pull effect. Moreover, compounds **3a–3p** display two or three maximum absorption peaks. Among them, the absorption peak at 280–400 nm is attributed to the π–π* transition from the aromatic rings in FBTD derivatives,[29] and the absorption peak at above 400 nm is assigned to the ICT of D–A–D systems.[30]

As depicted in Fig. 2b, Table 1 and Fig. S65, Table S5 (ESI†), the emission bands of **3a–3p** can range from 436 to 645 nm, covering the blue to red region, which makes full-color-tunable emission in the entire visible wavelength region to be realized. We further carefully analyzed the effect of different substituents (R) attaching to the 4,7-positions of the FBTD core to illustrate the full-color tunability of **3a–3p**. When R is trimethylsilyl and *n*-hexyl, the emission peaks of **3a** and **3b** are at 436 and 444 nm, respectively, showing blue fluorescence. When R is thienyl, phenyl, *p*-methylphenyl, *p*-methoxyphenyl, *p*-chlorophenyl, naphthyl and biphenyl, the maximum emission of **3c–3i** is located at 474 to 520 nm, showing blue-green or yellow-green fluorescence; when R is carbazolyl, TPA, *p*-CH_3O-TPA, and *p*-*N*,*N*-dimethylphenyl, the fluorescence peaks of **3j–3m** are red-shifted to the range from 582 to 643 nm, and the fluorescence color is orange or red. Generally, the emission wavelength of compounds **3a–3m** will be red-shifted with the increase of the electron-donating ability of the R group. Obviously, the fluorescence intensity of compound **3k** is greater than that of **3l** in THF (Table 1), which may be due to the presence of the OCH_3 group in **3l**, resulting in the increase of free rotation and non-radiative transition of **3l**.

Furthermore, the control compound **3n** is blue-shifted by 15 nm in comparison with **3m**, indicating that the fluorinated BTD can enhance the ICT effect.[21] In fact, the maximum emission is red-shifted as the degree of conjugate structure enlarges.[16] Nevertheless, the emission of **3o** (635 nm) is redder than that of **3n** (630 nm), suggesting that a linear triple bond may weaken the ICT effect in solution.[7] The monosubstituted compound **3p** is affected by the heavy atom effect (Br) and no fluorescence is observed.

The analysis of CIE chromaticity coordinates also intuitively shows that, by changing different substituents and adjusting the electron-donating intensity of the donor, the full-color-tunable of compounds **3a–3p** in solution can be realized (Fig. 2e).[9] Fortunately, most compounds (except **3l** and **3p**) have high Φ_F in THF, which facilitates the development of their applications in the solution state.

Likewise, as can be seen in Fig. 2c, f, Table 1 and Fig. S66 (ESI†), for compounds **3a–3p**, they exhibit full-visible color-tunable emission (445–672 nm) in the solid state. The dual-state fluorescence of compounds **3a–3p** has a basically consistent variation trend by regulating the push–pull electron strength of the R group. However, for each compound, especially for **3j–3m**, the solid-state emission has varying degrees of bathochromic shift relative to that in the solution state, which may be the formation of excimers and strong π–π interactions in the solid state.[29,31] Most of the compounds **3a–3p** have high Φ_F in the solid state (clearly, Φ_F, **3m** > Φ_F, **3n**), which helps to develop low-cost solid-state organic luminescent materials. Therefore, we further tested the fluorescence spectra of the thin film state prepared by mixing compounds **3a–3p** with poly(methyl methacrylate) (PMMA) and then dissolving them. As illustrated in Fig. 2d and g, Table 1 and Fig. S67 (ESI†), the films of **3a–3p** also exhibit the intense full-color emission covering the whole visible range.

In brief, compounds **3c–3k** have high fluorescence Φ_F and intense emission in both the solution and solid states, indicating that they are typical DSE fluorophores. These phenomena may be attributed to the delicate balance between the distorted conformation and rigid conjugation of compounds, which

Table 1 Photophysical data of compounds **3a–3p** in solution, solid and film states

	Solution (THF)					Solid			Film
Comp.	λ_{abs} (nm)	ε^a (10^4 M^{-1} cm^{-1})	λ_{em} (nm)	$\Phi_F{}^b$ (%)	Stokes shift (cm^{-1})	λ_{em} (nm)	$\Phi_F{}^b$ (%)	τ^c (ns)	λ_{em} (nm)
3a	278, 327, 365	18, 1.7, 1.5	436	59	4461	445	6.5	2.10	445
3b	276, 324, 370	5.0, 1.5, 1.2	444	84	4505	445	28	3.11	453
3c	281, 317, 424	3.9, 1.2, 1.1	511	85	4015	566	41	2.91	544
3d	278, 399	15, 2.6	475	84	4010	532	69	6.24	484
3e	279, 303, 410	18, 4.2, 3.4	493	89	4106	528	66	3.47	497
3f	279, 303, 427	16, 0.50, 0.43	519	93	4151	550	58	2.44	519
3g	279, 302, 400	13, 3.9, 3.1	474	84	3903	521	84	3.84	490
3h	279, 326, 432	5.7, 1.7, 1.9	514	57	3693	540	50	2.94	515
3i	315, 418	3.7, 3.1	501	89	3963	527	53	2.33	511
3j	320, 427	3.9, 2.8	582	61	6237	550	58	5.11	527
3k	279, 338, 484	18, 6.8, 5.6	628	41	4738	627	62	2.11	611
3l	279, 346, 503	5.3, 5.0, 4.1	409, 569	0.2	2306	672	23	2.11	628
3m	279, 327, 495	16, 5.0, 3.9	643	10	4650	663	20	2.02	625
3n	279, 325, 491	17, 4.3, 2.9	630	42	4494	660	2.2	1.05	607
3o	278, 315, 474	17, 2.6, 1.2	635	68	5349	662	4.6	2.04	625
3p	315, 448	2.7, 1.1	417, 530, 645	0.5	6818	638	1.5	1.46	599

[a] The molar absorption coefficient at absorption maxima. [b] The absolute quantum yield was obtained by using integrating spheres. [c] The fluorescence lifetime was obtained by double exponential fitting.

helps them activate emission and inhibit nonradiative transitions in both the solution and solid states.[32] Importantly, compounds **3c–3k** ($\Phi_{F,THF,solid}$ >40%) have higher quantum yields than some reported DSEgens.[24,33]

Solvatochromic effect. To explore the ICT properties of the D–A–D type fluorophores, we tested the fluorescence spectra of **3a–3p** in nine solvents with different polarities. As shown in Fig. 3a and b and Fig. S68–S75, Tables S6, S7 (ESI†), with the increase of solvent polarity, the maximum emission peaks of compounds **3a–3p** are red-shifted to varying degrees (19 nm to 135 nm), accompanied by significantly different fluorescence changes. Evidently, for **3a–3p**, they exhibit solvatochromism effects. And, especially for **3j–3p**, they are expected to be candidates for solvent polarity probes. Additionally, fluorinated **3m** has the greater solvatochromism effect than **3n**. And acetylene-containing **3n** is more remarkable than **3o**, respectively. Thus, the emission of compounds varies in sensitivity to solvent polarity, which may be connected to the strength of the ICT effect[30] and the magnitude of the dipole moment.[6]

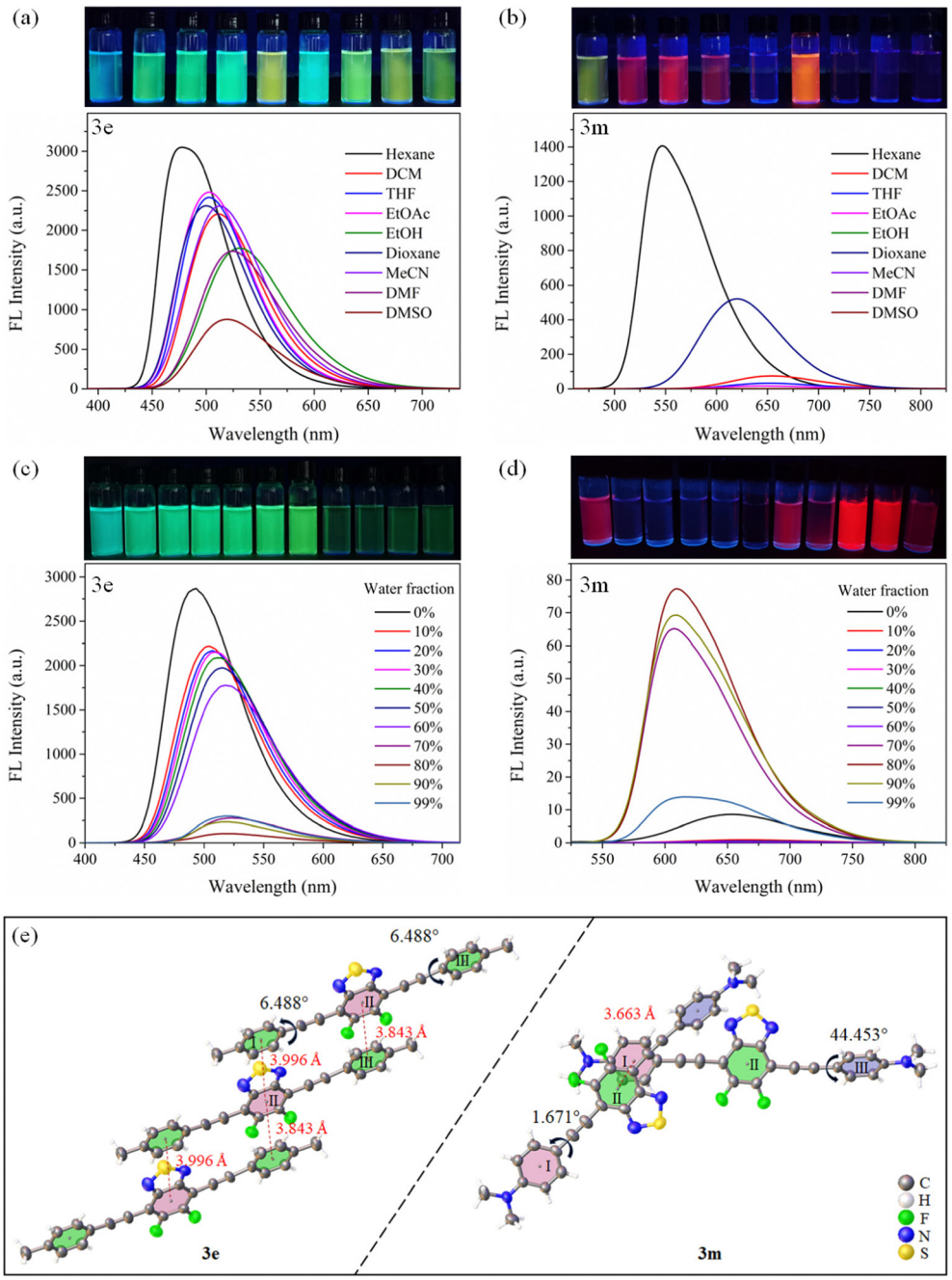

Fig. 3 (a) The fluorescence spectra and photographs of **3e** and (b) **3m** in various solvents. (c) The fluorescence spectra and photographs of **3e** and (d) **3m** in the THF/H_2O mixtures system. (e) The packing mode in the crystals of **3e** and **3m**.

Moreover, for compounds **3j–3p**, in a highly polar solvent (*i.e.*, EtOH, MeCN, DMF and DMSO), the fluorescence intensity is found to be significantly weakened. This may be due to the activation of rotation and vibration of the R group, thus enhancing the twisted ICT (TICT) effect and promoting the nonradiative transitions.[16]

Aggregation emission properties. Linking different R groups at 4,7-positions of FBTD may allow them to exhibit unique fluorescence properties in different aggregation states. Consequently, the emission spectra of compounds **3a–3p** in THF/H_2O systems were tested. As displayed in Fig. 3c and Fig. S76–S84, S89–S91 (ESI†), fluorophores **3a–3i** and **3n–3p** show bright fluorescence in pure THF as the solvent. When the water fraction (f_w) increases from 0% to 99%, the emission intensity gradually decreases, demonstrating an obvious ACQ effect. This may be due to that after decorating the R group on FBTD, the structures of **3a–3i** and **3n–3p** remain planar conjugated, resulting in their dominant π–π interactions in the aggregated state.

Further, as presented in Fig. 3d and Fig. S85–S88 (ESI†), when the f_w increases from 0% to 99%, the fluorescence intensity of compounds **3j–3m** first decreases sharply and then gradually increases. This suggests that, for **3j–3m**, they have the twisted ICT effect and remarkable AIEE properties.[34] Compounds **3j–3m** can exhibit the similar emission behavior to the hexaphenyl-benzene-based AIEEgens[34] or typical tetraphenylethene-based AIEgens.[35] Attaching rotors on FBTD, such as carbazole, TPA, *p*-OCH_3-TPA, and *p*-$N(CH_3)_2$-Ph, may give the molecule a highly distorted conformation, which restricts the motion of the R group in high f_w systems.[16] Interestingly, compounds **3m**, **3n** and **3o** have the same rotor, but the latter two compounds exhibit ACQ behavior, suggesting that the fluorinated BTD is beneficial for enhancing emission in the aggregated state. Thus, this study on these phenomena may provide a new perspective for the transition between ACQ and AIE or AIEE.[36]

To evaluate the AIEE effect of the compounds, their fluorescence spectra in ethanol/glycerol mixtures are tested by using **3m** and **3k** as examples. The red fluorescence of **3m** and **3k** can be markedly intensified with the increase of the glycerol fraction from 0% to 80% (Fig. S92, ESI†). This is due to that the increase of viscosity impedes the intramolecular rotations, thus inhibiting TICT progress and boosting the emission intensity.[37] Furthermore, as evidenced in Fig. S93 (ESI†), the level-off tails are noticed in the long-wave region with continuously increasing the f_w to 80% (or 70%). This interesting feature is caused by the light scattering effect, implying that the nanoaggregates are formed.[9,34] Indeed, the formation of nanoaggregates was confirmed by dynamic light scattering analyses (Fig. S94, ESI†).

Whether a compound can maintain stable and intense emission for a long time is important for its application development.[38] As demonstrated in Fig. S95 (ESI†), the fluorescence intensity of compounds **3a–3p** has no significant decrease after one hour of UV lamp irradiation, and three months of storage (powder at r.t., solution at 4 °C), indicating that they display excellent photostability.

DFT calculations and single crystal analysis

To elucidate the unique emission behavior of compounds **3a–3p** in solution, aggregate, and solid states, DFT calculations were used to study structure–property relationships (Tables S8–S23, ESI†).[8] As illustrated in Fig. S96 (ESI†), the LUMOs of compounds **3a–3p** are mainly distributed on the FBTD accepter core. Meanwhile, the HOMOs of **3a–3i** are predominantly located on the FBTD and R groups, but for **3j–3p**, the HOMOs are distributed over the R group. Usually, if the LUMO and HOMO can be effectively separated at both ends of the molecule, it is beneficial for the ICT process and improves the solvatochromism effect.[30] This is basically consistent with the above experimental data (Table S7, ESI†).

Moreover, the calculated energy gaps (ΔE) of compounds **3a–3p** are also presented in Fig. S96 (ESI†). It is found that ΔE can be modulated systematically from 3.32 to 2.05 eV by a rational combination of donor and acceptor units. In general, the absorption and emission peaks of compounds are red-shifted as the ΔE decreases.[8,39] The reason is that the ΔE is the narrower, the less excitation energy is required for the electron transition. DFT calculations show that compound **3a** has the largest ΔE, and the fluorescence data also confirm that **3a** has the shortest emission wavelength (Table 1). Meanwhile, there is a similar pattern between the ΔE value and maximum absorption.

Furthermore, the single crystal structures of **3e** and **3m** are analyzed to explore the reasons why they have different emission behaviors in the monomolecular and aggregate states.[25] As evidenced in Fig. 3e, compound **3e** is uniformly arranged in a parallel fashion. Among them, there is an obvious π–π interaction between the BTD core (II) and the benzene ring (I) or benzene ring (III). Meanwhile, the torsion angle between the II unit and the I or III ring is only 6.488°. Thus, **3e** shows the ACQ behavior.[1]

Nevertheless, there is a difference that **3m** is cross-stacked. Only the BTD core (II) and the benzene ring (I) have π–π interactions, and the torsion angles between the II unit and the I or III ring are 1.671° and 44.453°, respectively. Thus, its AIEE effect is ascribed to its distorted conformation and looser packing to restrict molecular motion and promote radiation transition.[1,34]

Interestingly, both the single crystal structure (Fig. S63, ESI†) and DFT results of **3c–3k** (Fig. S96, ESI†) show that FBTD and acetylene groups maintain linear conjugation, while R groups undergo varying degrees of torsion, which is the key to their DSE behavior.[32]

Bioimaging study of compound 3m

Compound **3m** has remarkable red emission and large Stokes shift, which give it the advantages of low tissue autofluorescence, high penetration depth and high contrast in cell imaging.[12,16] Therefore, 4T1 cells were selected as a model to study the ability of **3m** to image noninvasive in living cells. Firstly, different concentrations of **3m** solutions (*e.g.*, 10, 30, 60, 80 and 100 μg mL^{-1}) were prepared, and the further cytotoxicity

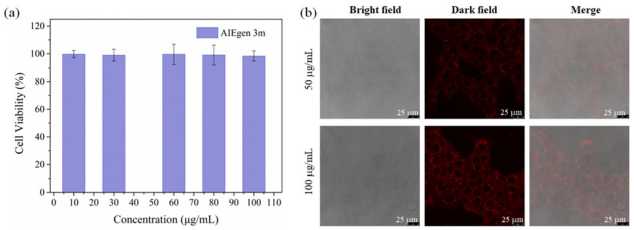

Fig. 4 (a) The biocompatibility of compound **3m**. (b) CLSM images of 4T1 cells incubated with **3m** of different concentrations (λ_{ex} = 405 nm and λ_{em} = 620–670 nm).

test was performed using the MTT method.[16] As depicted in Fig. 4a, compound **3m** with different concentrations can show excellent biocompability and low cytotoxicity on 4T1 cells. Especially, the 4T1 cells also display better viability at the same concentration and longer incubation time (48 h) compared to the reported work.[16,40]

Furthermore, the bioimaging study was evaluated by staining the 4T1 cells with the red-emissive **3m**. Confocal laser scanning microscopy (CLSM) images exhibit that dye **3m** gradually enters the cell after the incubation of 12 h, and the red fluorescence intensity is enhanced with the increase of the dye concentration (Fig. 4b). These clearly indicate that the FBTD derivative **3m** shows great potential for noninvasive imaging and real-time monitoring in live cells.[9]

Conclusions

In summary, we have successfully synthesized a series of D–A–D type full-color-tunable fluorophores **3a–3m** containing the same central fluorinated benzothiadiazole core and the control compounds **3n–3p**. Luminogens **3a–3p** show blue to red fluorescence in solution, solid and film states by regulating the electron-donating and electron-accepting strengths of moieties on both sides, and the color emission covering the whole visible range can be achieved as designed. Intriguingly, **3a–3p** reveal solvatochromism properties and large Stokes shifts, while **3c–3k** show DSE properties. Moreover, **3a–3i** and **3n–3p** display the ACQ effect, while **3j–3m** exhibit AIEE behavior by adjusting substituents. This means that, for compounds **3a–3p**, the DSE and the ACQ to AIEE conversion can be interestingly achieved. More importantly, red-emissive fluorophore **3m** can be utilized for live cancer cell staining. Thus, this work not only provides a new core skeleton for the design of full-color emission systems, but also expands their application in bioimaging.

Experimental section

All materials and reagents and solvents were purchased from commercial sources and used without further purification. Moreover, the ESI† provides details of chemicals and equipment.

By modifying the literature procedure,[25,26] FBTD derivatives **3a–3m** and control compounds **3n–3p** were successfully synthesized. All characterization data, such as ^{1}H, ^{13}C and ^{19}F NMR spectra as well as HRMS and single crystal data can be seen in the ESI.†

Author contributions

Si-Hong Chen: conceptualization, data curation, investigation, and writing – original draft. Xi-Ying Cao: validation, visualization, and writing – review and editing. Peng-Tao Hu: data curation, formal analysis, and writing – review and editing. Kai Jiang: conceptualization and writing – review and editing. Yong-Tong Liang: resources and writing – review and editing. Bing-Jia Xu: funding acquisition, methodology, and software. Zhong-Hao Li: resources and writing – review and editing. Zhao-Yang Wang: conceptualization, funding acquisition, project administration, supervision, and writing – review and editing.

Conflicts of interest

There are no conflicts to declare.

Acknowledgements

This work was supported by the Guangdong Basic and Applied Basic Research Foundation (No. 2021A1515012342 and 2023A1515010915), the Guangdong Provincial Science and Technology Project (No. 2017A010103016), and the Open Fund of Key Laboratory of Functional Molecular Engineering of Guangdong Province in SCUT (No. 2017kf01).

Notes and references

1 D. B. Zhao, G. C. Li, D. Wu, X. R. Qin, P. Neuhaus, Y. Y. Cheng, S. J. Yang, Z. Y. Lu, X. M. Pu, C. Long and J. S. You, Regiospecific N-heteroarylation of amidines for full-color-tunable boron difluoride dyes with mechanochromic luminescence, *Angew. Chem., Int. Ed.*, 2013, **52**, 13676.
2 M. L. Yang, I. S. Park and T. Yasuda, Full-color, narrowband, and high-efficiency electro-luminescence from boron and carbazole embedded polycyclic heteroaromatics, *J. Am. Chem. Soc.*, 2020, **142**, 19468.
3 H.-L. Xia, J. Zhang, J. C. Si, H. X. Wang, K. Zhou, L. Wang, J. B. Li, W. Sun, L. L. Qu, J. Li and X.-Y. Liu, Size- and emission-controlled synthesis of full-color luminescent metal-organic frameworks for tryptophan detection, *Angew. Chem., Int. Ed.*, 2023, **62**, e202308506.
4 K. F. Huang, H. Y. Qiu, X. T. Zhang, W. Luo, Y. Chen, J. C. Zhang, Y. H. Chen, G. N. Wang and K. Z. Zheng, Orthogonal trichromatic upconversion with high color purity in core-shell nanoparticles for a full-color display, *Angew. Chem., Int. Ed.*, 2023, **62**, e202218491.
5 L. Cao, M. H. Zan, F. M. Chen, X. Y. Kou, Y. L. Liu, P. Y. Wang, Q. Mei, Z. Hou, W. F. Li and L. Dong, Formation mechanism of carbon dots: From chemical structures to fluorescent behaviors, *Carbon*, 2022, **194**, 42.

6 Z. B. Wang, Z. X. Peng, K. Huang, P. Lu and Y. G. Wang, Butterfly-shaped π-extended benzothiadiazoles as promising emitting materials for white OLEDs, *J. Mater. Chem. C*, 2019, **7**, 6706.

7 Y. C. Wang, Y. Teng, H. Yang, X. Li, D. L. Yin and Y. L. Tian, Bioorthogonally applicable multicolor fluorogenic naphthalimide-tetrazine probes with aggregation-induced emission characters, *Chem. Commun.*, 2022, **58**, 949.

8 I. S. Park, S. Y. Lee, C. Adachi and T. Yasuda, Full-color delayed fluorescence materials based on wedge-shaped phthalonitriles and dicyanopyrazines: systematic design, tunable photophysical properties, and OLED performance, *Adv. Funct. Mater.*, 2016, **26**, 1813.

9 Z. Chen, H. Qin, Y. Yin, D. D. Deng, S. Y. Qin, N. Li, K. Wang and Y. Sun, Full-color emissive D–D–A carbazole luminophores: Red-to-NIR mechano-fluorochromism, aggregation-induced near- infrared emission, and application in photodynamic therapy, *Chem. – Eur. J.*, 2023, **29**, e202203797.

10 S. Munan, S. Kottarathil, M. M. Joseph, A. Jana, M. Ali, K. Mapa, K. K. Maiti and A. Samanta, IndiFluors: a new full-visible color-tunable donor-acceptor-donor (D1–A–D2) fluoro-phore family for ratiometric pH imaging during mitophagy, *ACS Sens.*, 2023, DOI: **10.1021/acssensors.1c02381**.

11 H. Gu, W. J. Liu, H. D. Li, W. Sun, J. J. Du, J. L. Fan and X. J. Peng, 2,1,3-Benzothiadiazole derivative AlEgens for smart phototheranostics, *Coord. Chem. Rev.*, 2022, **473**, 214803.

12 B. A. D. Neto, J. R. Correa and J. Spencer, Fluorescent benzothiadiazole derivatives as fluorescence imaging dyes: a decade of new generation probes, *Chem. – Eur. J.*, 2022, **28**, e202103262.

13 J.-N. Chang, J.-W. Shi, Q. Li, S. Li, Y.-R. Wang, Y.-F. Chen, F. Yu, S.-L. Li and Y.-Q. Lan, Regulation of redox molecular junctions in covalent organic frameworks for H_2O_2 photosynthesis coupled with biomass valorization, *Angew. Chem., Int. Ed.*, 2023, **62**, e202303606.

14 S. J. Wu, D. M. Ren, K. Zhou, H. L. Xia, X. Y. Liu, X. T. Wang and J. Li, Linker engineering toward full-color emission of UiO-68 type metal-organic frameworks, *J. Am. Chem. Soc.*, 2021, **143**, 10547.

15 J.-X. Wang, Y. Wang, M. Almalki, J. Yin, O. Shekhah, J. T. Jia, L. Gutiérrez-Arzaluz, Y. D. Cheng, O. Alkhazragi, V. K. Maka, T. K. Ng, O. M. Bakr, B. S. Ooi, M. Eddaoudi and O. F. Mohammed, Engineering metal-organic frameworks with tunable colors for high-performance wireless communication, *J. Am. Chem. Soc.*, 2023, **145**, 15435.

16 C. C. Liu, H. T. Bai, B. Z. He, X. W. He, J. Y. Zhang, C. Chen, Y. P. Qiu, R. Hu, F. X. Zhao, Y. X. Zhang, W. He, J. H. C. Chau, S. J. Chen, J. W. Y. Lam and B. Z. Tang, Functionalization of silk by AIEgens through facile bioconjugation: Full-color fluorescence and long-term bioimaging, *Angew. Chem., Int. Ed.*, 2021, **60**, 12424.

17 R. H. Xu, W. J. Chi, Y. Z. Zhao, Y. Tang, X. N. Jing, Z. Wang, Y. Zhou, Q. F. Shen, J. Zhang and Z. W. Yang, All-in-one theranostic platforms: Deep-red AIE nanocrystals to target dual-organelles for efficient photodynamic therapy, *ACS Nano*, 2022, **16**, 20151.

18 Z. L. Yu, Y. Yu, J. X. Jiang, L. Q. Qin and D. H. Hu, Fluoro substitution effect on 2,1,3-benzothiadiazole-based hybridized local and charge transfer state fluorophores for high-performance organic light-emitting diodes, *Dyes Pigm.*, 2023, **213**, 111184.

19 J. Hu, Q. Li, X. D. Wang, S. Y. Shao, L. X. Wang, X. B. Jing and F. S. Wang, Developing through-space charge transfer polymers as a general approach to realize full-color and white emission with thermally activated delayed fluorescence, *Angew. Chem., Int. Ed.*, 2019, **58**, 8405.

20 T. R. Li, J. L. Miao, C. Y. Xu, Y. Nie, W. Liu, Y. X. Li, G. N. Liu and X. C. Jiang, One F atom matters: synthesis, aggregation-induced emission and stimuli-responsiveness of three isomers of fluoro/formyl substituted tetraphenylethene derivatives, *J. Mater. Chem. C*, 2022, **10**, 8657.

21 C. B. Li, G. Y. Jiang, J. Yu, W. W. Ji, L. X. Liu, P. F. Zhang, J. Du, C. L. Zhan, J. G. Wang and B. Z. Tang, Fluorination enhances NIR-II emission and photothermal conversion efficiency of phototheranostic agents for imaging-guided cancer therapy, *Adv. Mater.*, 2023, **35**, 2208229.

22 Q. S. Shi, Y. Y. Ni, L. M. Yang, L. Kong, P. Y. Gu, C. Y. Wang, Q. H. Zhang, H. P. Zhou and J. X. Yang, Fluorination of naphthalimide-cyanostilbene derivatives to achieve dual-state emission luminogens with strong fluorescence in highly polar environments for bioimaging, *J. Mater. Chem. B*, 2023, **11**, 6859.

23 S. Das, P. P. Das, J. W. Walton, C. K. Quah, K. Ghoshal and M. Bhattacharyya, Aggregation-induced emission switch showing high contrast mehanofluorochromism and solvatofluorochromism: Specifically detects HSO_3^- in bioimaging studies, *Dyes Pigm.*, 2023, **217**, 111413.

24 Z. Huang, A. X. Ding, J. X. Yang, C. Y. Wang and F. Tang, Conjugating coumarin with tetraphenylethylene to achieve dual-state emission for reversible mechanofluorochromism and live cell imaging, *Chem. – Eur. J.*, 2023, e202203628.

25 S.-H. Chen, S.-H. Luo, L.-J. Xing, K. Jiang, Y.-P. Huo, Q. Chen and Z.-Y. Wang, Rational design and facile synthesis of dual-state emission fluorophores: expanding functionality for the sensitive detection of nitroaromatic compounds, *Chem. – Eur. J.*, 2022, **28**, e202103478.

26 J. Wang, H. Y. Cui, H. P. Ruan, Y. Zhao, Y. Zhao, L. Zhang and X. P. Wang, The Lewis acid induced formation of a stable diradical with an intramolecular ion pairing state, *J. Am. Chem. Soc.*, 2022, **144**, 7978.

27 L.-Y. Xi, R.-Y. Zhang, S. Liang, S.-Y. Chen and X.-Q. Yu, Copper-catalyzed aerobic synthesis of 2-aryl- pyridines from acetophenones and 1,3-diaminopropane, *Org. Lett.*, 2014, **16**, 5269.

28 Y. G. Hu, Y. Q. Gao, J. H. Ye, Z. Q. Ma, J. T. Feng, X. L. Liu, P. Lei and M. Szostak, Suzuki-Miyaura cross-coupling of 2-pyridyl trimethylammonium salts by N–C activation catalyzed by air- and moisture-stable Pd-NHC precatalysts: Application to the discovery of agrochemicals, *Org. Lett.*, 2023, **25**, 2975.

29 T. Patten, N. Graw, S. Friedl, D. Stalke and A. Krawczuk, An investigation of solid-state emission of halogenated diphenyl phosphanyl anthracenes, *Adv. Opt. Mater.*, 2023, **11**, 2202753.

30 F. Zhao, J. Y. Zhao, H. T. Liu, Y. Wang, J. X. Duan, C. L. Li, J. Q. Di, N. Zhang, X. Y. Zheng and P. K. Chen, Synthesis of π-conjugated chiral organoborane macrocycles with blue to near-infrared emissions and the diradical character of cations, *J. Am. Chem. Soc.*, 2023, **145**, 10092.

31 N. Konig, Y. Godinez-Loyola, F. S. Yang, C. Laube, M. Laue, P. Lonnecke, C. A. Strassert and E. Hey-Hawkins, Facile modification of phosphole-based aggregation-induced emission luminogens with sulfonyl isocyanates, *Chem. Sci.*, 2023, **14**, 2267.

32 A. Huber, J. Dubbert, T. D. Scherz and J. Voskuhl, Design concepts for solution and solid-state emitters - a modern viewpoint on classical and non-classical approaches, *Chem. – Eur. J.*, 2023, **29**, e202202481.

33 D. Zou, Z. H. Li, D. Long, X. Dong, H. Qu, L. L. Yang and X. Y. Cao, Molecular cage with dual outputs of photochromism and luminescence both in solution and the solid state, *ACS Appl. Mater. Interfaces*, 2023, **15**, 13545.

34 S. Pramanik, H. Deol, V. Bhalla and M. Kumar, AIEE active donor acceptor donor-based hexaphenylbenzene probe for recognition of aliphatic and aromatic amines, *ACS Appl. Mater. Interfaces*, 2018, **10**, 12112.

35 Y. F. Zuo, J. K. Liu, P. Li, K. Li, J. W. Y. Lam, D. C. Wu and B. Z. Tang, Full-color-tunable AIE luminogens for 4D code, security patterns, and multicolor LEDs, *Cell Rep. Phys. Sci.*, 2023, **4**, 101202.

36 S.-H. Chen, J.-M. Xu, Y.-M. Li, B.-R. Peng, L.-Y. Luo, H.-Y. Feng, Z.-H. Chen and Z.-Y. Wang, Research progress of aggregation-caused quenching (ACQ) to aggregation-induced emission (AIE) transformation based on organic small molecules, *Chin. J. Org. Chem.*, 2022, **42**, 1651.

37 C. Wang, W. C. Jiang, D. Tan, L. Huang, J. Li, Q. L. Qiao, P. Yadav, X. G. Liu and Z. C. Xu, Monitoring amyloid aggregation via a twisted intramolecular charge transfer (TICT)-based fluorescent sensor array, *Chem. Sci.*, 2023, **14**, 4786.

38 Y. Y. Qi, X. S. Cao, Y. Zou and C. L. Yang, Multi-resonance organoboron-based fluorescent probe for ultra-sensitive, selective and reversible detection of fluoride ions, *J. Mater. Chem. C*, 2021, **9**, 1567.

39 A. Nina-Diogo, B. Bertrand, S. Thorimbert, G. Gontard, S. Nassem-Kahn, A. Echeverri, J. Contreras-Garcia, C. Allain, G. Lemercier, E. Luppi and C. Botuha, 3-Hydroxypyridinyl- substituted-1,2,4-triazoles as new ESIPT based fluorescent dyes: Synthesis and structure-fluorescence properties correlations, *Adv. Opt. Mater.*, 2023, **11**, 2300336.

40 P. K. Mehta, J. Y. Lee, E. T. Oh, H. J. Park and K. H. Lee, Ratiometric fluorescence sensing system for lead ions based on self-assembly of bioprobes triggered by specific Pb^{2+}-peptide interactions, *ACS Appl. Mater. Interfaces*, 2023, **15**, 14131.